Chemical Science

Accepted Manuscript

This article can be cited before page numbers have been issued, to do this please use: M. Chosenyah, M. Rohullah, V. Avulu, K. V. J. Jose and R. Chandrasekar, *Chem. Sci.*, 2026, DOI: 10.1039/D6SC01977C.

ROYAL SOCIETY OF CHEMISTRY

rsc.li/chemical-science

View Article Online
DOI: 10.1039/D6SC01977C

COMMUNICATION

A Chameleon-like Core-Shell Organic/Lanthanide Flexible Crystal Waveguide for Bandwidth and Colour Tunability

Received 00th January 20xx,
Accepted 00th January 20xx

DOI: 10.1039/x0xx00000x

Melchi Chosenyah,[a] Mehdi Rohullah,[a] Avulu Vinod Kumar,[a] K. V. Jovan Jose,*[a] and Rajadurai Chandrasekar*[a]

Optical fibers capable of dynamically generating and/or transporting narrow/broadband spectral signals in the visible spectral region based on input, much like how a chameleon changes its color, is quintessential for developing visible light communication devices. Here, we demonstrate a mechanically flexible, blue-violet fluorescent, 2-(4,4'-bis(2,6-di(1H-pyrazol-1-yl)pyridin-4-yl)biphenyl) (BPP) crystal waveguide surface coordinated to red fluorescent Eu(tta)$_3$. The BPP microcrystal waveguide acting as core, with BPP-Eu(III) as shell, provides a hybrid platform for broad and narrow band signal transmission. Depending on the input light and the absorption of the core or shell, the crystal acts as an active-active, active-passive, or passive-passive light-generating and/or transporting optical waveguide. Notably, the pseudo-plasticity of the core-shell hybrid waveguide enables modulation of signal output direction without compromising the optical performances. The development of such smart optical waveguides has enormous potential for visible light communication and selective light-based micro precision sensing applications.

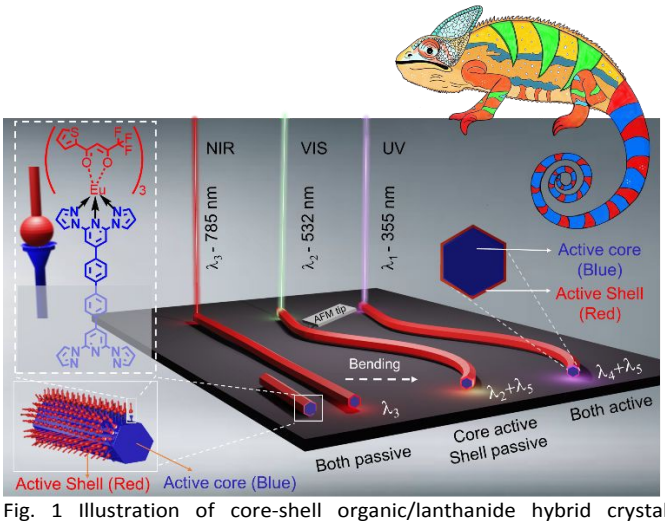

Fig. 1 Illustration of core-shell organic/lanthanide hybrid crystal waveguide showing active/passive input-dependent optical waveguiding.

Chameleon-like crystalline waveguides that can selectively generate and transport light across the blue-to-NIR spectrum with tunable bandwidth hold significant promise for advancing visible light communication (VLC) technologies.[1,2] Unlike silicon or silicon-based complementary metal oxide semiconductor materials,[2] organic waveguides offer active and passive optical waveguides depending on whether the input optical signal is within or away from the molecule's absorption window.[3-17] We have previously demonstrated that the microcrystals of 2-(4,4'-bis(2,6-di(1H-pyrazol-1-yl)pyridin-4-yl)biphenyl) (BPP) serves both passive and active waveguides while exhibiting mechanical compliance.[17,18] Active[4,5,7-16] and passive[3,5,6,16] organic waveguides, when combined with energy transfer and reabsorption properties, can be utilized to create various optical components such as directional couplers,[5,19] add-drop filters,[20] wavelength division multiplexers,[21,22] and photonic circuits.[5,18-25]

Numerous one-dimensional (1D) organic crystalline waveguides transporting visible light have been demonstrated.[26-33] Additionally, several core-shell strategy for organic optical waveguides have been reported.[15,34-42] However, spontaneous generation and propagation of narrow and/or broadband optical signals invoking active/passive transduction, and sensitized energy transfer in a single organic waveguide remains challenging. Typically, organic crystals exhibit broadband emission, while lanthanides display narrow band *f-f* transitions. Recently, X. -D. Wang *et al.* reported a core-

[a] School of Chemistry and Centre for Nanotechnology, University of Hyderabad, Prof. C. R. Rao Road, Gachibowli, Hyderabad 500046, Telangana, India.
Supplementary Information available: [details of any supplementary information available should be included here]. See DOI: 10.1039/x0xx00000x

View Article Online
DOI: 10.1039/D6SC01977C

COMMUNICATION

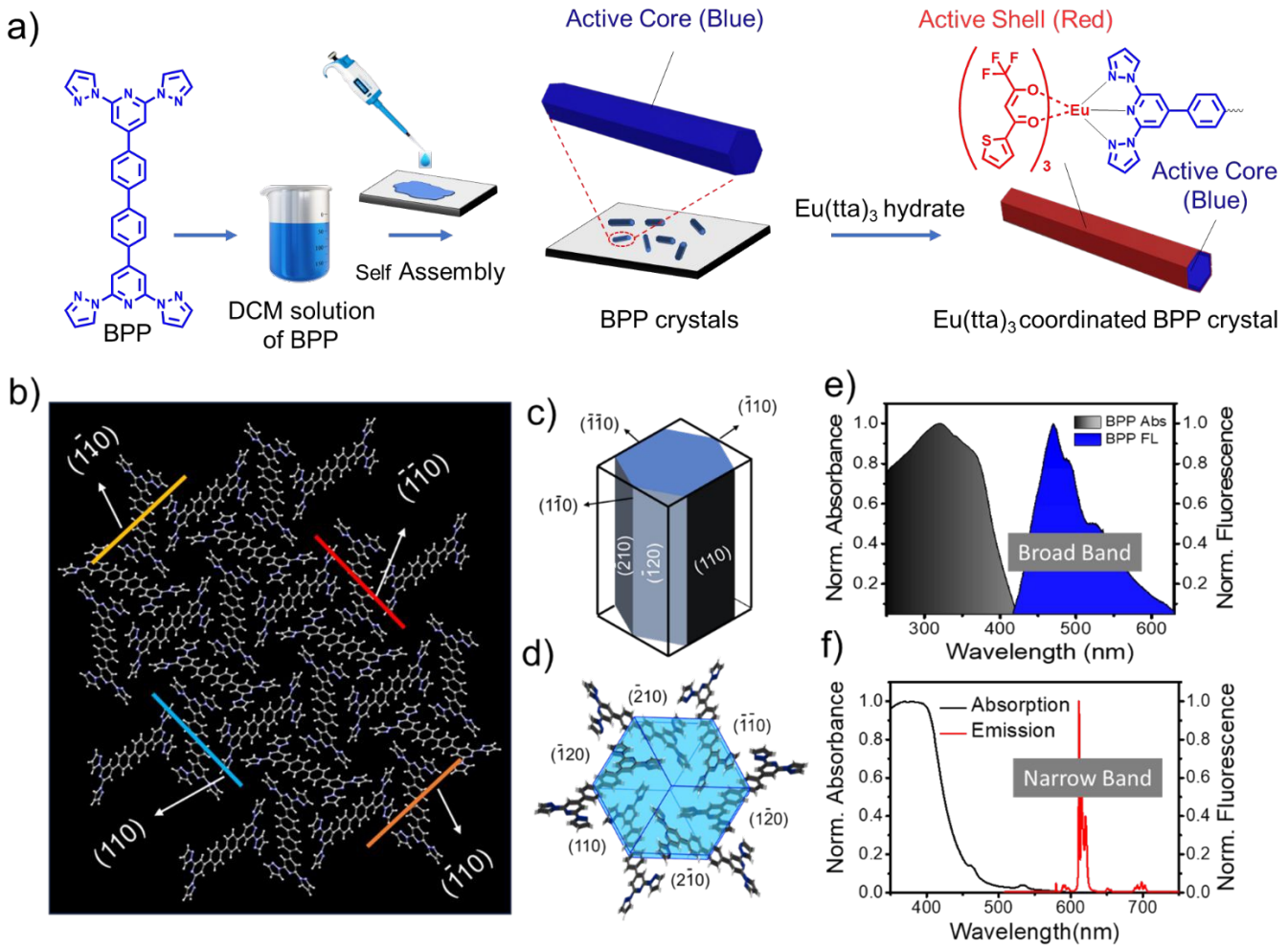

Fig. 2 (a) Schematic elucidation of the formation of core-shell organic/lanthanide hybrid hexagonal microcrystals in DCM via supramolecular self-assembly. (b) Single crystal X-ray structure depicting the molecular packing of rectangular-shaped BPP crystal with corresponding facets. (c) Facets of hexagonal BPP crystals. (d) Growth morphology of the BPP crystal. (e) Solid-state absorption and emission spectra of BPP ligand. (f) Solid-state absorption and emission spectra of $Eu(tta)_3$ hydrate.

shell strategy to coat the rigid nanocrystal surface with a suitable organic acceptor or donor molecules, thereby modifying the broadband active emission properties of the crystals.[9,12,15] Nevertheless, developing a chameleon-like optical waveguide capable of generating and transporting (i) dynamic colours across the visible spectral regions, (ii) either narrowband or broadband signals, and (iii) a combination of narrow and broad bands presents a significant challenge. This task necessitates the layering of organic and lanthanide optical materials. A viable chemical approach to achieve this desired goal involves selecting a mechanically flexible, microcrystal derived from an organic fluorescent (FL) ligand. This microcrystal can then be coordinatively reacted at the surface with an appropriate lanthanide metal to form an organic-lanthanide core-shell hybrid optical waveguide (Fig. 1).

Apart from BPP crystal's active/passive waveguiding propensity[17,18] and mechanical flexibility,[18] its unexplored chemical feature is the available tridentate 2,6-bispyrazolylpyridine unit. For example, $Ln(tta)_3$ hydrates (tta: thenoyltrifluoroacetonate) can react with BPP ligands to produce a nine-coordinated narrowband luminescent lanthanide complex.[43-47] Here, we demonstrate an innovative "coordination chemistry at the crystal surface" strategy to fabricate organic/lanthanide core-shell hybrid optical waveguides from blue-violet FL BPP microcrystals. The exposed tridentate sites at the BPP microcrystal's surface selectively and coordinatively react with red-FL $Eu(tta)_3$ hydrate. The obtained core-shell hybrid optical waveguide selectively transduces broadband blue-violet emission from the organic ligand (the unreacted core), narrow band red emission from the Eu(III) of

shell, or purple colour results from mixing blue and red colours depending upon the optical absorbance of the input-light (Fig.S1). For a UV laser input, the waveguide's core and shell actively produce and guide the broad blue-violet band and narrow red band signals, respectively. On the other hand, the waveguide core and shell passively and actively guide narrow laser and red signals, respectively, for the 532 nm input. For 785 nm input, both core and shell passively guide the laser light. Further, the mechanical flexibility of BPP crystals provides additional prospects for manipulating optical signals. Thus, illustrating a futuristic, flexible, organic/lanthanide hybrid crystal optical waveguide technology delivering active/passive tunable light output. This chameleon-like behaviour to dynamically adjust the signal output for different inputs makes these waveguides versatile for sensing and circuit application.

The BPP molecule was synthesized using the reported procedure.[46] The microrods of BPP were obtained by slow evaporation of 50 μL BPP solution (c ≈ 0.35×10^{-3} M) in dichloromethane (DCM) at room temperature (Fig. 2a). Further, to increase the rod's length, 1 mL of DCM solvent was added to the previous solution and self-assembled to observe longer microrods under a confocal optical microscope. Here, some rods act as nucleation sites, facilitating molecular assembly on the rod's growth axes to increase the rod's lengths. The self-assembled one-dimensional microstructures exhibited hexagonal and rectangular cross-sections, and their characteristics were examined in field emission scanning electron microscopy (FESEM) (Figs. S1, S2). The exposure of BPP ligands on the surface of the hexagonal microcrystals was investigated by analyzing the planes of the rectangular macrocrystal. This analysis revealed that the (110), (-210), and (-120) planes of the hexagonal microcrystals were exposed (Fig. 2b,c). From these identified planes, it is evident that the tridentate ligands are presented on the surface of the BPP's hexagonal microcrystals (Fig. 2d).

The crystalline microrod's solid-state optical absorption spans from UV to 425 nm, with a maximum absorption of 320 nm. The BPP showed blue-violet FL in the solid state, which extends from ≈ 400 to 650 nm with λ_{max} at 470/490/526 nm (Fig. 2e). The optical absorption of $Eu(tta)_3$ hydrate falls in the UV region and extends up to 600 nm, whereas it emits sensitized red FL (580-700 nm) from the hypersensitive $^5D_0$-^7F_J (J = 0-4) transitions of the Eu(III) ion (Figs. 1f, S3a). Interestingly, the emission of BPP and absorption of $Eu(tta)_3$ overlap facilitating radiative energy transfer from ligand to metal ion. This energy transfer enables enhance of red emission intensity from the Eu(III) (Fig. S3b,c).

To test the coordination chemistry-assisted surface coating of $Eu(tta)_3$ on the BPP crystal surface, a hexane solution (20 μL) of $Eu(tta)_3$ hydrate (c ≈ 0.115×10^{-3} M) was dropped on the BPP crystals. Here, the exposed tridentate ligand available at the crystal surface drives the water molecules out of $Eu(tta)_3$ hydrate, forming a thin layer of 2,6-bispyrazolylpyridine-$Eu(tta)_3$ coordination complex on the BPP crystal surface. The FESEM image established crystal structural integrity even after Eu(III) complex formation at the crystal surface (Fig. S4a,b). Optical waveguiding studies further validated the presence of BPP-$Eu(tta)_3$ complexation (Fig. S4c-f). The energy dispersive X-ray analysis (EDX) confirmed the Eu content (Fig. S4g). The selected area electron diffraction (SAED) obtained via transmission electron microscopy (TEM) showed distinctive

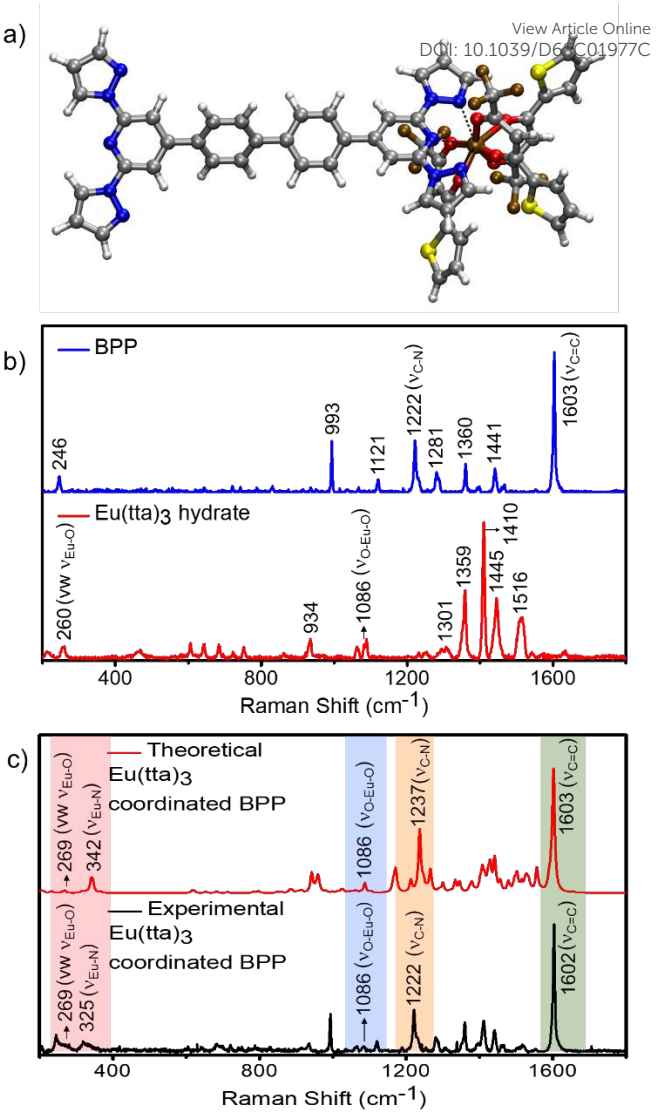

Fig. 3 (a) Energy optimized structure of $Eu(tta)_3$ coordinated to BPP. (b) Micro Raman spectra of BPP and $Eu(tta)_3$ hydrate. (c) Theoretical (B3LYP level of theory with Def2svp basis set, using the Gaussian09 suite of programs) and experimental Raman spectra of $Eu(tta)_3$ coordinated BPP. Excitation wavelength λ_{ex} = 785 nm.

diffraction patterns from BPP and Eu-coordinated heterostructure (Fig. S5). Additionally, the Raman spectra of the hexagonal rods of BPP ligand, those reacted with nine-coordinated Eu(III) complex and pure $Eu(tta)_3$ hydrate, have demonstrated new peaks and peak shifts that support the presence of a layer of Eu complex on the surface (Fig. 3a-c). Furthermore, because of the formation of a thin inorganic layer around the BPP microcrystal, the signal intensities of BPP dominate over those originating from the thin layer of the Eu complex. Increasing the concentration of $Eu(tta)_3$ hydrate will in turn enhance the Eu-centered emission intensity (Figure S6). The far-IR region of the spectra exhibited a new asymmetric peak with a base width of about 298-365 cm^{-1}. The peak asymmetry is due to the contribution of two types of $\nu_{(Eu-N)}$ in the experimental spectrum. Moreover, the calculated Raman spectrum also showed a new peak for $\nu_{(Eu-N)}$ = 342 cm^{-1}, confirming the coordination of BPP with $Eu(tta)_3$ (Fig. 3c). The 1603 cm^{-1} peak in BPP and the 1086 cm^{-1} peak in the $Eu(tta)_3$ hydrate are observed both in the experimental and calculated

View Article Online
DOI: 10.1039/D6SC01977C

COMMUNICATION

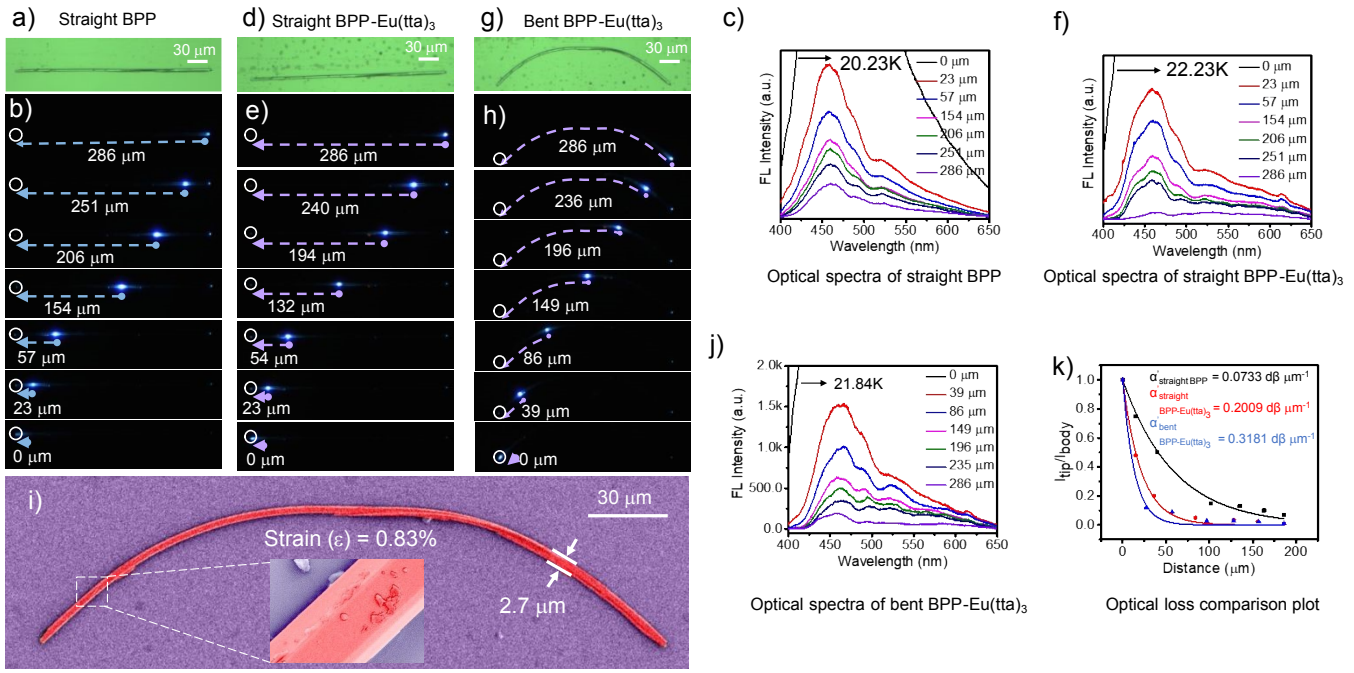

Fig. 4 Confocal optical image and FL images of BPP microcrystals in (a,b) uncoordinated, (d,e) Eu(tta)$_3$ coordinated (straight), (g,h) Eu(tta)$_3$ coordinated (bent) configurations. The excitation position-dependent FL spectra obtained in the (c) uncoordinated BPP, (f) straight Eu(tta)$_3$ coordinated BPP, and (j) bent Eu(tta)$_3$ coordinated BPP microcrystals. (i) Color-coded FESEM micrograph of coordinated BPP microcrystal with Eu(tta)$_3$ hydrate. Inset: magnified image of hexagonal morphology. (k) The plot of I_{tip}/I_{body} vs. Distance used for the optical loss coefficient calculation for uncoordinated, coordinated straight, and coordinated bent BPP microcrystals.

spectra with different intensities. The 246 cm^{-1} peak of BPP and 260 cm^{-1} peak ($\nu_{(Eu\text{-}O)}$) of Eu(tta)$_3$ hydrate merged in the experimental spectra giving rise to an asymmetric peak. These results confirmed the formation of BPP-Eu(tta)$_3$ coordination complex on the surface of BPP microcrystals.

To understand the mechanophotonic properties of hybrid microstructure, a BPP crystal ($L \approx 286$ μm) was selected and the optical waveguiding studies were performed (Fig. 4a,b). A 405 nm continuous-wave (CW) laser was focused onto one end of the microcrystal from the bottom to provide excitation. The produced blue-violet FL was collected from the opposite end of the microcrystal. The excitation position was systematically varied along the length of the microcrystal while maintaining a fixed collection position at one end. The corresponding spectra were plotted in Fig. 4c. The optical loss coefficient, α' (a parameter to estimate the waveguiding efficiency) of the optical waveguide was calculated to be α' = 0.0733 dB μm^{-1} by fitting the plot of I_{tip}/I_{body} vs. distance between excitation and collection position (Fig. 4k). The same microcrystal's surface was treated with Eu(tta)$_3$ hydrate to form a nine-coordinated Eu(III)-BPP complex as a thin layer (Figs. 4d,e,f). The FL spectrum recorded at the laser irradiation point/opposite terminal revealed two bands corresponding to the BPP ligand at 450 nm (broadband), as well as the Eu complex around 630 nm (narrowband) region (Figs. 4f, S4d). Thereby, confirming the presence of the Eu complex (Shell) on top of the microcrystal (core) due to the formation of a hybrid organic/lanthanide heterostructure. The optical waveguiding studies performed on the core-shell crystal confirmed the dual signal propagation (λ_{max} of 450 nm from BPP and 630 nm from Eu) to terminals (Fig. 4f) with α' of 0.2009 dB μm^{-1} (Fig. 4k).

Later, the confocal microscope attached with an atomic force microscope (AFM) cantilever tip was used to investigate the micromechanical compliance of the hybrid heterostructure waveguide. For that, the left terminal of the hybrid waveguide was gently pushed with the cantilever tip by applying a force in the forward direction, which confirmed the crystal's flexibility. Later, a similar force was applied on the right terminal by implementing the same procedure, resulting in a bow-shaped curved hybrid waveguide (Fig. 4g-l). This mechanical bending imparted a strain of 0.83% on the hybrid waveguide (Fig. S7). The FESEM image of the hybrid waveguide revealed a thickness of 2.7 μm (Fig. 4i). Despite the strain due to mechanical bending, the hybrid waveguide obtained from an elastically flexible BPP microtube did not revert to its original shape after applied stress removal because of its pseudo-plasticity[19] (owing to crystal surface and substrate adhesive interaction the elastic microcrystal behaves akin to plastic). The strained hybrid waveguide was subjected to a 355 nm laser to investigate its

View Article Online
DOI: 10.1039/D6SC01977C

COMMUNICATION

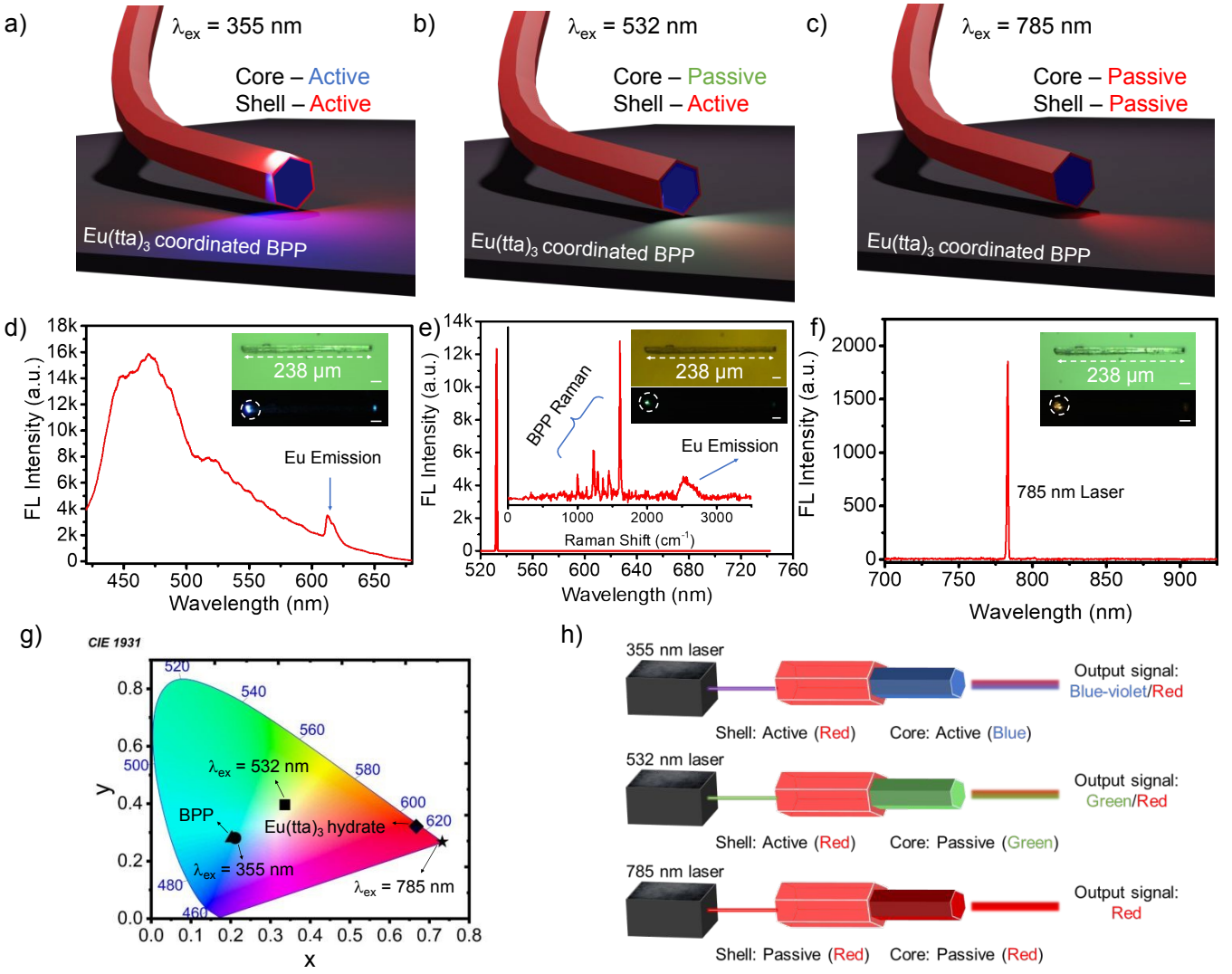

Fig. 5 Graphical representation of the dynamic performance of Eu(tta)$_3$ coordinated BPP hybrid crystal waveguide for the excitation with (a) 355 nm, (b) 532 nm, (c) 785 nm laser. FL spectrum collected at the left tip, when excited the crystal with (d) 355 nm (e) 532 nm (f) 785 nm laser (Inset: confocal and FL images of the crystal with the excitation of 355, 532 and 785 nm lasers, respectively). Scale bar: 20 μm (g) The CIE 1931 diagram depicts the colour coordinates for BPP, Eu(tta)$_3$ hydrate, Eu(tta)$_3$ coordinated BPP when irradiated with different wavelength lasers. (h) Graphical representation of the light transduction mechanisms and output colours for different lasers.

optical waveguiding characteristics. As expected, the strained hybrid waveguide showed a slightly higher optical loss of 0.3181 dB μm^{-1} attributed to the crystal bending and scattering loss (Fig. 4k).

To showcase the intended generation of multiple spectral colours, bandwidths, and transportability within the core-shell, a 238 μm -long hybrid crystal waveguide, was specifically chosen (Fig. 5a, inset of 5d). Illuminating the left end of the hybrid crystal waveguide with either 355 nm lasers resulted in FL, due to optical absorption from both BPP and Eu(III) and their propagation to the opposite end of the waveguide (Fig. 5a,d). Here, both core and shell act as active waveguides. Conversely, when the same waveguide was excited with a 532 nm laser at one end, only the red FL from the Eu complex was actively transduced to the other end, given that its absorption region aligned well with the excitation source (Fig. 5b,e). In contrast, the absorption of BPP molecules ends at 440 nm, enabling passive guidance of the 532 nm green light (Figs. S3c, S8). In addition to the red FL from the Eu, BPP's Raman signals were observed. This led to the creation of a dual-mode active-passive light transduction through core and shell, respectively within the hybrid crystal waveguide.

View Article Online
DOI: 10.1039/D6SC01977C

Further, experimentation involved the excitation of the same hybrid crystal waveguide with a 785 nm light, situated away from the absorption bands of both BPP and Eu(III), at one of its terminals (Fig. 5c,f). Consequently, the same laser light passively propagated to the other end of the hybrid microcrystal, confirming the passive-only light transportability of core and shell of the hybrid crystal waveguide (Fig. 5c,f). The graphical representation in Figure 5h summarizes the optical performance of the constructed hybrid crystal waveguide, outlining the signal outcome based on the input laser source. The CIE diagram visually illustrates the emission changes for each recorded output. (Figure 5g,h, Table. S1)

Conclusions

In conclusion, we have successfully demonstrated the optical waveguiding capabilities of highly flexible hybrid organic/lanthanide core-shell crystals, exhibiting chameleon-like dynamic colour-changing properties. This work not only showcases advancements in flexible organic-inorganic crystal optical waveguides but also emphasizes the untapped potential of crystals with metal ligation features. The crystals of BPP-$Eu(tta)_3$ hybrid structure successfully guided blue-violet and red active-active signal with a 355 nm laser, green and red passive-active signal with a 532 nm laser, and red passive signal with a 785 nm laser with low optical loss and showed its versatile input-dependent waveguiding nature. Such hybrid materials composed of organic/inorganic wavelength-tunable active/passive type; flexible hybrid crystal waveguides are exemplary materials for advancing organic photonic technologies. Such exemplary photonic structures transducing combined broadband and narrowband optical signals is necessary for VLC technologies.

Author contributions

The manuscript was written with contributions from all authors. All authors have approved the final version of the manuscript.

Acknowledgment

R.C. thanks SERB (STR/2022/00011 and CRG/2023/003911), and DST/INT/RUS/RSF/P-71/2023(G) for funding. M.C. thanks CSIR for the fellowship.

Conflicts of interest

There are no conflicts to declare.

References

1 S. N. Ismail, M. H. Salih, *AIP Conference Proceedings*, 2020, **2213**, 020289.
2 A. Khapre, J. Hazarika, R. Chandrasekar, *Nat. Commun.,* 2025, **16**, 10862.
3 Y. Su, Y. Zhang, C. Qiu, X. Guo, L. Sun, *Adv. Mater. Technol.,* 2020, **5**, 1901153.
4 Y. S. Zhao, *Organic Nanophotonics: Fundamentals and Applications*, Springer, Berlin, 2014.
5 R. Chandrasekar, *Mechanophotonics for Organic Photonic Integrated Circuits*, IOP Publishing, London, 2024.
6 S. Basak, R. Chandrasekar, *J. Mater. Chem. C.,* 2013, **2**, 1404.
7 K. Takazawa, Y. Kitahama, Y. Kimura, G. Kido, *Nano Lett.,* 2005, **5**, 1293-1296.
8 F. Hu, G. Zhang, C. Zhan, W. Zhang, Y. Yan, Y. Zhao, H. Fu, D. Zhang, *Small,* 2014, **11**, 1335-1344.
9 J. -X. Zhang, S. Zhao, Z. Lu, and X. -D. Wang, *Adv. Funct. Mater.,* 2025, **35**, e06412.
10 T. Matsuo, J. Kuwabara, T. Kanbara, S. Hayashi, J. Phys. *Chem. Lett.,* 2023, **14**, 29, 6577-6582.
11 M. Zhuo, Y. Tao, X. Wang, Y. Wu, S. Chen, L. Liao, L. Jiang, *Angew. Chem. Int. Ed.,* 2018, **130**, 11470-11474.
12 S. Chen, M. -P. Zhuo, X. -D. Wang, G. -Q. Wei, L. -S. Liao, *PhotoniX,* 2021, **2**, 2.
13 M. -P. Zhuo, X. -Y. Fei, Y. -C. Tao, J. Fan, X. -D. Wang, W. -F. Xie, L. -S. Liao, *ACS Appl. Mater. Interfaces,* 2019, **11**, 5298-5305.
14 Z. -Z. Li, J. -J. Wu, X. -D. Wang, K. -L. Wang, S. Zhang, W. -F. Xie, L. -S. Liao, *Adv. Opt. Mater.,* 2019, **7**, 1900373.
15 J. -H. Jiang, S. Zhao, J. -X. Zhang, Z. -J. Lv, J. Song, Y. Sun, L. -S. Liao, X.-D. Wang, *Nano Lett.,* 2024, DOI 10.1021/acs.nanolett.4c03330.
16 M. Annadhasan, S. Basak, N. Chandrasekhar, R. Chandrasekar, *Adv. Opt. Mater.,* 2020, **8**, 2000959.
17 N. Chandrasekhar, M. A. Mohiddon, R. Chandrasekar, *Adv. Opt. Mater.,* 2012, **1**, 305-311.
18 A. V. Kumar, M. Rohullah, M. Chosenyah, J. Ravi, U. Venkataramudu, R. Chandrasekar, *Angew. Chem. Int. Ed.,* 2023, **62**, e202300046.
19 M. Annadhasan, A. R. Agrawal, S. Bhunia, V. V. Pradeep, S. S. Zade, C. M. Reddy and R. Chandrasekar, *Angew. Chem. Int. Ed.,* 2020, **59**, 13852.
20 A. V. Kumar, E. Mamonov, T. Murzina, R. Chandrasekar, *Adv. Opt. Mater.,* 2023, **11**, 2201507.
21 A. V. Kumar, M. Godumala, J. Ravi, R. Chandrasekar, *Angew. Chem. Int. Ed.,* 2022, **61**, e202212382; *Angew. Chem.,* 2022, **134**, e202212382.
22 R. E. R. -Noriega, F. D. S. -Pinedo, M. C. -Arenas, J. V. Urbina, H. E. H. -Figueroa, A. Lakhtakia, *Opt. Eng.,* 2025, **64**, 077103.
23 C. Zhang, C.-L. Zou, Y. Zhao, Y. Zhao, C.-H. Dong, C. Wei, H. Wang, Y. Liu, G.-C. Guo, J. Yao, Y. S. Zhao, *Sci. Adv.,* 2015, **1**, e1500257.
24 A. V. Kumar, M. Rohullah, M. Chosenyah, G. Sindhuja, R. Chandrasekar, *Angew. Chem. Int. Ed.,* 2025, **64**, e202502122.
25 M. Rohullah, M. Chosenyah, A. V. Kumar, R. Chandrasekar, *Small,* 2025, **21**, 2407498.
26 H. Liu, Z. Lu, B. Tang, C. Qu, Z. Zhang, H. Zhang, *Angew. Chem. Int. Ed.,* 2020, **59**, 12944.
27 S. Hayashi, S.-y. Yamamoto, D. Takeuchi, Y. Ie, K. Takagi, *Angew. Chem. Int. Ed.,* 2018, **57**, 17002.
28 K. Takazawa, J.-i. Inoue, K. Mitsuishi, T. Kuroda, *Adv. Funct. Mater.,* 2013, **23**, 839.
29 S. Hayashi, T. Koizumi, *Angew. Chem. Int. Ed.,* 2016, **55**, 2701-2704.
30 M. -P. Zhuo, J. -J. Wu, X. -D. Wang, Y. -C. Tao, Y. Yuan, L. -S. Liao, *Nat. Commun.,* 2019, **10**, 3839.
31 M. -P. Zhuo, Y. Su, Y. -K. Qu, S. Chen, G. -P. He, Y. Yuan, H. Liu, Y. -C. Tao, X. -D. Wang, L. -S. Liao, *Adv. Mater.,* 2021, **33**, 2102719.
32 Q. Lv, X. -D. Wang, Y. Yu, M. -P. Zhuo, M. Zheng, L. -S. Liao, *Nat. Commun.,* 2022, **13**, 3099.
33 B. Yin, J. Gu, M. Feng, G. C. Zhang, Z. Zhang, J. Zhong, C. Zhang, B. Wen, Y. S. Zhao, *Nanoscale,* 2019, **11**, 7111-7116.
34 B. Wu, M.-P. Zhuo, Y.-L. Shi, L.-F. Gu, Y.-D. Zhao, Y. Su, Y.-Y. Li, H. Lu, W.-F. Li, Z.-S. Wang, X.-D. Wang, *Chem,* 2025, **11**, 102497.

View Article Online
DOI: 10.1039/D6SC01977C

35 S. Zhao, J.-X. Zhang, L. Wang, C.-F. Xu, Y.-X. Ma, X.-D. Wang, L.-S. Liao, *J. Am. Chem. Soc.,* 2025, **147**, 15510-15518.
36 L. Lan, L. Li, J. Qi, X. Pan, Q. Di, P. Naumov, H. Zhang, *Nat. Commun.,* 2023, **14**, 7582.
37 S. Liu, L. Lan, H. Zhang, Chem. Sci., 2025, 16, 18919-18927.
38 X. Yang, L. Lan, X. Pan, Q. Di, X. Liu, L. Li, P. Naumov, H. Zhang, Nat. Commun., 2023, 14, 2287.
39 K. Liu, Y. Lei, H. Fu, *Chem. Mater.,* 2020, **32**, 5162-5172.
40 Y. Lei, Y. Sun, Y. Zhang, H. Zhang, H. Zhang, Z. Meng, W.-Y. Wong, J. Yao, H. Fu, *Nat. Commun.,* 2018, **9**, 4358.
41 C. Feng, Z. Xu, X. Wang, H. Yang, L. Zheng, H. Fu, *ACS Appl. Mater. Interfaces.,* 2017, **9**, 7385-7391.
42 S. Basak, R. Chandrasekar, *Adv. Funct. Mater.,* 2010, **21**, 667–673.
43 D. J. Strohecker, V. M. Lynch, B. J. Holliday, R. A. Jones, *Dalton Trans.,* 2017, **46**, 7733-7742.
44 J. M. Stanley, X. Zhu, X. Yang, B. J. Holliday, *Inorg. Chem.,* 2010, **49**, 2035.
45 S. Basak, Y. S. L. V. Narayana, M. Baumgarten, K. Müllen, R. Chandrasekar, *Macromolecules,* 2013, **46**, 362-369.
46 N. Chandrasekhar, R. Chandrasekar, *Chem. Commun.,* 2010, **46**, 2915.
47 Y. S. L. V. Narayana, R. Chandrasekar, *ChemPhysChem,* 2011, **12**, 2391-2396.

View Article Online
DOI: 10.1039/D6SC01977C

The supporting data has been provided as part of the Supplementary information.